Hardening of fcc hard-sphere crystals by introducing nanochannels: Auxetic aspects

Jakub W. Narojczyk [1,*], Konstantin V. Tretiakov [1,2], Jerzy Smardzewski [3], and Krzysztof W. Wojciechowski [1,2,†]

[1]*Institute of Molecular Physics, Polish Academy of Sciences, M. Smoluchowskiego 17, 60-179 Poznań, Poland*

[2]*Uniwersytet Kaliski im. Prezydenta Stanisława Wojciechowskiego, Wydział Politechniczny, Katedra Informatyki, Nowy Świat 4, 62-800 Kalisz, Poland*

[3]*Department of Furniture Design, Faculty of Forestry and Wood Technology, Poznan University of Life Sciences, Wojska Polskiego 28, 60-637 Poznań, Poland*

Tailoring the materials for a given task by modifying their elastic properties is attractive to material scientists. However, recent studies of purely geometrical atomic models with structural modifications showed that designing a particular change to achieve the desired elastic properties is complex. This work concerns the impact of nanochannel inclusions in fcc hard sphere crystal on its elastic properties, especially auxetic ones. The models containing six nanochannel arrays of spheres of another diameter, oriented along the [110]-direction and its symmetric equivalents, have been studied by Monte Carlo simulations in the isothermal-isobaric (NpT) ensemble using the Parinello-Rahman approach. The inclusions have been designed such that they do not affect the cubic symmetry of the crystal. The elastic properties of three different models containing inclusions of various sizes are investigated under four thermodynamic conditions. We find that six nanochannels filled with hard spheres of larger diameter increase system stiffness compared with the fcc crystal without nanoinclusions. The current finding contrasts the recently reported results [J.W. Narojczyk *et al.* Phys. Status Solidi B **259**, 2200464 (2022)], where the fcc hard sphere crystal with four nanochannels shows reduced stiffness compared to the system without nanoinclusions. Moreover, the six nanochannel models preserve auxetic properties in contrast to the fcc hard sphere crystal with four nanochannel arrays, which loses auxeticity.

I. INTRODUCTION

Auxetics [1,2]—materials with the negative Poisson's ratio [3]—draw increasing attention among scientists and materials engineers. Despite the intense studies over the past thirty years, our understanding of their nature and the number of their actual practical applications could still be improved. Not long after the early reports in the mid-1980s about mechanical model structures exhibiting negative Poisson's ratio [4,5], the manufacture of materials with such extraordinary properties was made possible, and the first theoretical model of a thermodynamically stable phase with this counter-intuitive behavior was provided [6–8]. After decades of research that followed, the auxetic properties have been reported in cubic crystals [9–14], foams [1,15,16], polymers [2,17,18], and composites [19–21], as well as in specifically engineered structures [22–24], nanostructures [25,26], or metamaterials [27–32]. Moreover, significant effort has been put into developing various auxetic fabrics [33] for personal applications. Along with the experimental studies, the theoretical models exhibiting negative Poisson's ratio [34–36] help in the understanding of the auxeticity mechanism and the creation of new auxetic systems. Noteworthy examples are the well-known models by Grima *et al.*, which have negative Poisson's ratio due to the effects of rotating rigid [37] or semirigid units [38]. Apart from purely theoretical [19,34,37,39–41] or experimental [42–44]

studies, one should notice the essential role of computer modeling in auxetic research. These can be roughly divided into continuum methods [45] (finite element methods) and atomic models. The atomic models are beneficial in explaining the origin of auxeticity in natural crystals [9] and basic model systems (such as hard and soft sphere crystals [46,47]). They also allow us to study the impact of structure modification at the microlevel on elastic properties [48,49].

The hard sphere crystal model plays an essential role in the theory of liquids and condensed matter physics due to the anharmonicity of the interactions and its athermal nature [50,51]. The elastic properties of the hard spheres crystal have been the subject of many studies [46,52–58]. In 1987, Runge and Chester [53] found that the fcc hard sphere solid at melting density exhibits the negative Poisson's ratio in the [110][1̄10]-direction equal to −0.054(9), and according to the modern classification, it is a partially auxetic system [10]. It was later found that the Poisson's ratio of the fcc hard spheres crystal, in the close packing limit, in the [110][1̄10]-direction is −0.072(1) [47].

Controlling the auxetic properties of the system by modifying the structure can be essential in creating materials with predetermined elastic properties. Given that the hard sphere crystal is partially auxetic, this system is suitable for examining the influence of purely geometrical factors on elastic properties, particularly, the auxetic properties. Recently, the impact of structural modification on the atomic level, in the form of multiple periodic arrays of nanochannels filled by hard spheres of another diameter than those forming crystals and oriented in different directions in hard sphere crystals has

*narojczyk@ifmpan.poznan.pl
†kww@ifmpan.poznan.pl

been studied [59–62]. Those studies showed that designing a structural modification to achieve the desired elastic properties is difficult. An fcc crystal of hard spheres containing a periodic array of identical nanochannel inclusions, oriented along one of the principal crystallographic directions (e.g., the [001]-direction), showed a significant decrease of the negative Poisson's ratio (as low as −0.87) when inclusions are filled with the larger diameter spheres [59]. It is worth noting that such a low Poisson ratio was observed in a crystal where introduced nanoinclusions caused the loss of cubic symmetry. Additionally, further studies have shown that an array of tripled nanochannels, oriented in three mutually orthogonal directions ([100], [010], and [001]) [60,61] or quadrupled nanochannels oriented in [111]-direction and its equivalent ones [62], preserve the cubic symmetry of the crystal. Still, one observes a substantial increase in Poisson's ratio. Moreover, partially auxetic properties observed in pure fcc hard sphere crystal have been weakened or lost. The difficulty in predicting the influence of microscopic modifications on macroscopic elastic properties encourages us to design and investigate the cubic symmetry system with six nanochannels.

This work's primary goal is to study the elastic properties of hard sphere crystals comprised of six periodic nanochannel arrays, each oriented along the [110]-direction and the equivalent ones. Particularly, we study the influence of introducing inclusions in the form of nanochannels filled by hard spheres of another diameter then the spheres forming fcc hard sphere crystal on the auxetic properties of the crystal. Beyond the cognitive aspect, studies of such models may be interesting from a practical point of view. The rapid development of nanotechnology allows us to expect manufacturing of metamaterials at the nanoscale, e.g., by atomic layer deposition [63]. Thus, in the not far future, one can expect the fabrication of materials with nanoinclusions.

The article has the following structure. In Sec. II, the studied model has been described. Section III provides basic information on the research methodology. In Sec. IV the results have been discussed. The summary and conclusions have been placed in Sec. V.

II. MODELS

The considered models comprise N spheres that form the face-centered cubic lattice and interact through a hard potential

$$\beta u_{ij} = \begin{cases} \infty, & r_{ij} < \sigma_{ij}, \\ 0, & r_{ij} \geqslant \sigma_{ij}, \end{cases} \quad (1)$$

where r_{ij} denotes the distance between centres of spheres i and j, σ_{ij} is the sum of the radii of spheres, $\beta = 1/(k_B T)$, k_B is the Boltzmann constant, and T is the temperature. We consider three systems with periodic supercells containing inclusions presented in Fig. 1. Inclusions are six differently sized nanochannels oriented in the [110]-direction and the equivalent ones. Each nanochannel is filled by spheres within a cylindrical volume designated around a selected crystallographic axis, with a radius of this cylinder denoted as r_c. For small r_c values, only the spheres lying directly on the channel's axis form the inclusion, as shown in Fig. 1—the system with supercell C0, where the inclusion spheres are
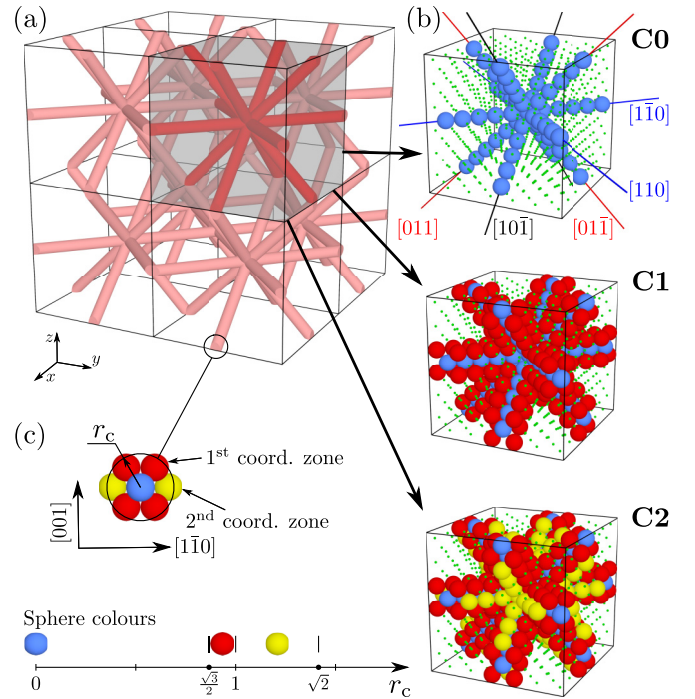

FIG. 1. The structures of studied systems with inclusions in the form of nanochannels in the [110]-direction and its symmetric equivalents. (a) The investigated structure with eight supercells where red cylinders schematically represent nanochannels. (b) Supercell structures: the hard spheres forming crystals (green points) are artificially scaled down to show the topology of inclusions; the colored spheres belong to the nanochannels. (c) The radius r_c is shown on the cross section of the channel, together with spheres lying on the axis of the nanochannel (blue), in the first coordination zone (red), and the second coordination zone (yellow).

marked in blue. As the value of r_c increases, the nearest neighbor spheres, colored in red in Fig. 1, are also included in the nanochannel, and we obtain the system with supercell C1. With the further increse of r_c, the next nearest neighbors (yellow spheres) are also added to the channels, see Fig. 1(c), and one obtains the system with supercell C2. Further, we will refer to the systems with these three sizes of inclusions as the crystals with supercells C0, C1, and C2. All the inclusion spheres are identical but differ in their diameters from the ones forming the base crystal. The sphere diameter of the crystal is equal to σ, and the diameter of channel spheres is equal to $\sigma' \neq \sigma$. Each of the described systems will be parametrized by the ratio σ'/σ, also referred to as the diameter scaling factor. For example, for a crystal's sphere diameter of $\sigma = 1.0$ and inclusion sphere diameter of $\sigma' = 1.01$, the scaling factor equals 1.01, and 0.98 for $\sigma' = 0.98$. The studied systems with inclusions contain different numbers of spheres (N_{inc}) that constitute the inclusion. Parameters of the studied structures have been gathered in Table I.

III. COMPUTATIONAL DETAILS

The free enthalpy change corresponding to a thermodynamically reversible elastic deformation under external

TABLE I. The inclusion parameters for the C0, C1, and C2 systems. The number of inclusion spheres (N_{inc}) in systems of $N = 864$ (corresponding to $6 \times 6 \times 6$ fcc unit cells) and systems of $N = 6912$ (corresponding to $12 \times 12 \times 12$ fcc unit cells).

Cx	$r_c[\sigma]$	N_{inc} ($N = 864$)	N_{inc} ($N = 6912$)
C0	$<\sqrt{3}/2$	64	512
C1	<1	256	2048
C2	$<\sqrt{2}$	346	2768

pressure (p) reads [64],

$$\Delta G = \frac{V_p}{2} \sum_{ijkl}^{3} B_{ijkl} \varepsilon_{ij} \varepsilon_{kl}, \tag{2}$$

where B_{ijkl} are the elastic constants at constant pressure, ε_{ij} are the components of the (Lagrange) strain tensor, V_p is the volume of the equilibrium (reference) state at p, and $ijkl$ are x, y, z.

The Monte Carlo (MC) computer simulations, based on the Parrinello-Rahman approach [64–66], allow us to calculate the elastic properties of studied systems within the isothermal-isobaric ensemble (NpT). According to the Parrinello-Rahman method, the box matrix $\mathbf{h}$ and the reference box matrix $\mathbf{h}_p$ can be used to express the Lagrange strain tensor [66],

$$\boldsymbol{\varepsilon} = \frac{1}{2} \left(\mathbf{h}_p^{-1} . \mathbf{h} . \mathbf{h}_p^{-1} - \mathbf{I} \right), \tag{3}$$

where $\mathbf{I}$ is a unit matrix, $\mathbf{h}$ and $\mathbf{h}_p$ (for convenience) are assumed to be symmetric. The rows/columns of the box matrix correspond to the edge vectors of the simulation box. The reference matrix $\mathbf{h}_p$ is the average value of the $\mathbf{h}$ matrix at equilibrium under pressure p, $\mathbf{h}_p \equiv \langle \mathbf{h} \rangle$. Here and further, $\langle ... \rangle$ is the average in the NpT ensemble, calculated as

$$\langle f \rangle = \frac{\int d\varepsilon^{(6)} f \exp(-\beta G)}{\int d\varepsilon^{(6)} \exp(-\beta G)}. \tag{4}$$

The elastic compliance tensor is calculated from fluctuations of the strain tensor for the system under pressure [64]

$$S_{ijkl} = \beta V_p \langle \Delta \varepsilon_{ij} \Delta \varepsilon_{kl} \rangle, \tag{5}$$

where $V_p = |\det(\mathbf{h}_p)|$ is the volume of the system at equilibrium (reference) state at p, and $\Delta \varepsilon_{ij} = \varepsilon_{ij} - \langle \varepsilon_{ij} \rangle$.

The elastic constants B_{ijkl} are related to the elastic compliances S_{ijkl} by the equation [67]

$$\sum_{n,m} S_{ijmn} B_{mnkl} = \frac{1}{2} (\delta_{ik}\delta_{jl} + \delta_{il}\delta_{jk}), \tag{6}$$

where δ_{ij} is the Kronecker delta.

In particular, for cubic symmetry, the Gibbs free energy can be written as follows:

$$\begin{aligned} \Delta G = &\frac{1}{2} B_{11} V_p \left(\varepsilon_{xx}^2 + \varepsilon_{yy}^2 + \varepsilon_{zz}^2 \right) \\ &+ B_{12} V_p \left(\varepsilon_{xx}\varepsilon_{yy} + \varepsilon_{yy}\varepsilon_{zz} + \varepsilon_{xx}\varepsilon_{zz} \right) \\ &+ 2 B_{44} V_p \left(\varepsilon_{xy}^2 + \varepsilon_{yz}^2 + \varepsilon_{xz}^2 \right), \end{aligned} \tag{7}$$

where Voigt's notation used the indices 1–6 to replace xx, yy, zz, yz, xz, and xy, respectively.

The Poisson's ratio for a selected pair of $\vec{\mathbf{n}}$ and $\vec{\mathbf{m}}$ (mutually orthogonal directions) can be obtained in the following way [68]:

$$\nu_{nm} = -\frac{m_i m_j S_{ijkl} n_k n_l}{n_p n_r S_{prst} n_s n_t}, \tag{8}$$

where n and m indicate two directions. $\vec{\mathbf{n}}$ is the direction of the applied stress, and $\vec{\mathbf{m}}$ is the direction in which the system's reaction to the applied stress is measured. The n_i and m_j are their respective direction cosines. More details regarding the calculations of elastic properties have been given in the Ref. [64]. Monte Carlo simulations in NpT ensemble were performed for systems consisting of $N = 864$ and $N = 6912$ particles in periodic boundary conditions. One should notice that in the Monte Carlo method, when performing simulations in the NpT ensemble with varying box shape, two extremes can be applied regarding the box motions. First, the box trial motions can accompany any trial motion of a particle. Second, they can be done after each cycle, i.e. after trial motions of all the particles in the box. In this work the standard MC scheme [51] with the typical Metropolis algorithm based on two kinds of trial motions was used. The first kind is the changes in the sphere positions, and the second one is the changes in the components of the symmetric box matrix ($\mathbf{h}$). The acceptance ratio for both types of movements was close to 40%, and the changes of the components of the symmetric box matrix have been attempted $\sqrt{N}$ times less frequently than the spheres' motions.

The hard sphere crystals with three types of supercells, C0, C1, and C2, and with different sizes of the nanochannel's spheres (with σ' between 0.95σ and 1.07σ) were studied at the dimensionless pressures $p^* = p\beta\sigma^3 = 50, 100, 250$, and 1250. Only stable cubic structures have been considered. Thus, the range of σ'/σ for obtained results varies depending on the system type and pressure. One hundred independent simulation runs have been performed for each pair of σ'/σ and p^* values. Each run took 10^7 MC cycles for systems $N = 864$, from which the first 10^6 cycles were discarded from further analysis (treated as the period to reach the thermodynamic equilibrium). For systems composed of $N = 6912$, the length of a single simulation run has been increased by eight times to 8×10^7 MC cycles. This extended the simulation time for a single run to approximately eight weeks of CPU time.

IV. RESULTS AND DISCUSSION

The introduction of inclusions into the crystal structure impacts the system's geometry for any $\sigma' \neq \sigma$. (When $\sigma' = \sigma$, one has the case of the pristine fcc hard sphere crystal.) This has been illustrated in the plots in Fig. 2, where the components of the box matrix $\mathbf{h}$ have been plotted with respect to the scaling factor σ'/σ. The figure shows that an increase of σ'/σ and inclusion size leads to the larger values of diagonal components (h_{11}, h_{22}, and h_{33}) of the box matrix. In addition, $h_{11} = h_{22} = h_{33}$ and the values of off-diagonal elements of the matrix are zero within the accuracy of the calculations (the bottom row of Fig. 2). That suggests systems with inclusions may retain cubic symmetry.
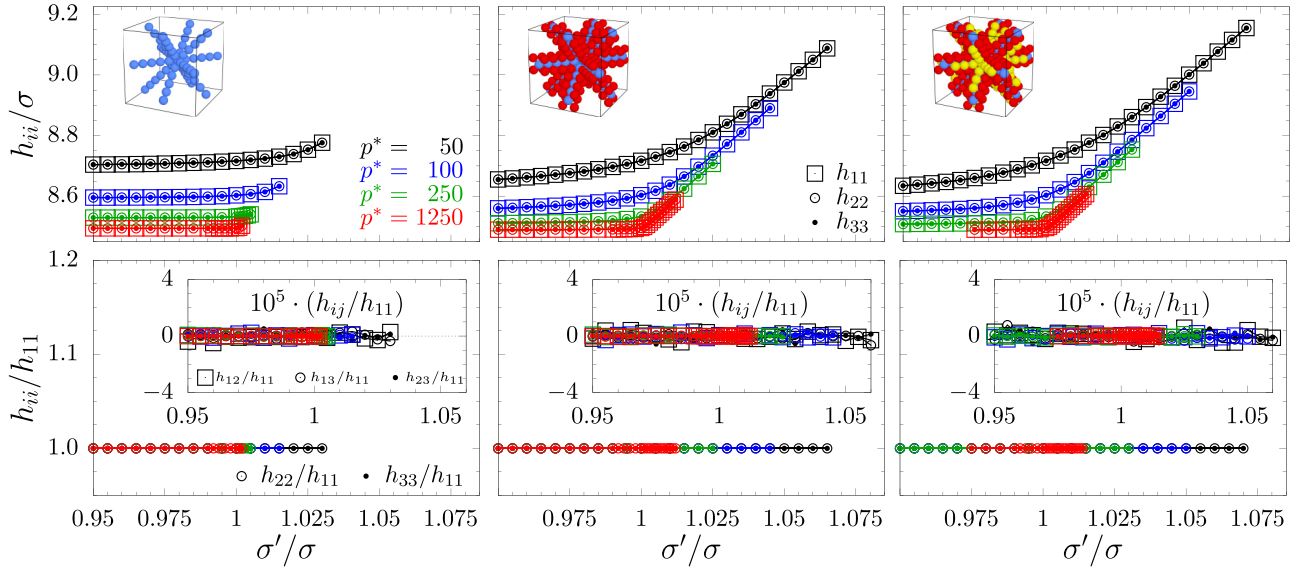
FIG. 2. The diagonal box matrix components h_{ii} (top row) plotted with respect to σ'/σ. Ratios of the diagonal and off-diagonal **h** components (bottom row). The data for corresponding pressure values have been indicated with colors. Data for different inclusion sizes have been organized in three columns for C0 (left), C1 (center), and C2 (right). This convention for colors and column arrangement is kept throughout the paper.

A. Elastic properties of systems with six nanochannels

Figure 3 presents all the components of the elastic constant matrix **B** for all studied systems at various thermodynamical conditions. It is important to note that all the required relations for the cubic symmetry [69] are satisfied. As shown in Fig. 3, the $B_{ii} = B_{jj}$ holds for $i, j = 1, 2, 3$ and separately for $i, j = 4, 5, 6$, and $B_{12} = B_{k3}$ is true for $k = 1, 2$. The remaining elements of the elastic constant matrix equal zero within the range of computational accuracy. As a result, we observe three nonzero components of the elastic constant matrix, B_{11}, B_{12}, and B_{44}, characteristic of cubic symmetry. Thus, the elastic constant matrix is given in the following form:

$$\mathbf{B} = \begin{bmatrix} B_{11} & B_{12} & B_{12} & 0 & 0 & 0 \\ B_{12} & B_{11} & B_{12} & 0 & 0 & 0 \\ B_{12} & B_{12} & B_{11} & 0 & 0 & 0 \\ 0 & 0 & 0 & B_{44} & 0 & 0 \\ 0 & 0 & 0 & 0 & B_{44} & 0 \\ 0 & 0 & 0 & 0 & 0 & B_{44} \end{bmatrix}. \quad (9)$$

Figure 3 shows that for all studied pressures, the values of the elastic constants increase with the size of the particles constituting the nanoinclusion in the range $\sigma'/\sigma > 1$. In addition, the dependences of the elastic constants on the scaling factor (σ'/σ) have similar behavior for different pressures and differ only quantitatively.

The dependences of the Poisson's ratio in the main crystallographic directions on σ'/σ are shown in Fig. 4(a). Poisson's ratio has the lowest value for a system without inclusions, i.e., pristine hard spheres crystal. The presence of spheres with another diameter in the system leads to an increase in Poisson's ratio. Since the considered systems are anisotropic, the values of Poisson's ratio will differ depending on the choice of $\vec{n}$ and $\vec{m}$ directions. Presenting the full range of PR

values for each system in one plot is not feasible. However, it is possible to present extreme Poisson's ratios for different $\vec{n}$ directions. Figure 4(b) presents the maximum and minimum values of Poisson's ratios in spherical coordinates at $p^* = 50$ for different scaling factors (σ'/σ). An increase in the Poisson's ratio in any direction is observed at $\sigma'/\sigma \neq 1$ for all studied systems (C0, C1, and C2).

It should be noted that a finite-size effect (the dependence of the obtained results on the size of the studied system) was negligible. Figure 4 clearly shows that the results for the system $N = 864$ particles and $N = 6912$ particles are in good agreement.

B. Elastic properties of system with six nanochannels vs system with four nanochannels

Considering that the dependences of the elastic constants (Fig. 3) and Poisson's ratios (Fig. 4) on the scaling factor (σ'/σ) are respectively similar for different pressures, further discussion was carried out for the pressure $p^* = 50$ as a typical case. The elastic constants of system C1 with six nanochannels at $p^* = 50$ and the analogous system C1 with four nanoinclusions (in the [111]-direction and equivalent ones, studied recently [62]) as a function of σ'/σ are presented in Fig. 5. Comparison of elastic constants of systems with six and four nanochannels reveals the entirely different character of their behavior with respect to the scaling factor. For the systems with six nanochannels at $\sigma'/\sigma > 1$, an enhancement of the stiffness of hard sphere crystals due to the introduction of nanochannels in the [110]-direction and equivalent ones is observed. Oppositely, for the system with four nanochannels in the [111]-direction and equivalent ones at $\sigma'/\sigma > 1$, we see the decrease in B_{11} and B_{44} values. For $\sigma'/\sigma < 1$ in both cases, all elastic constants have the same dependences on σ'/σ, and the values of the corresponding
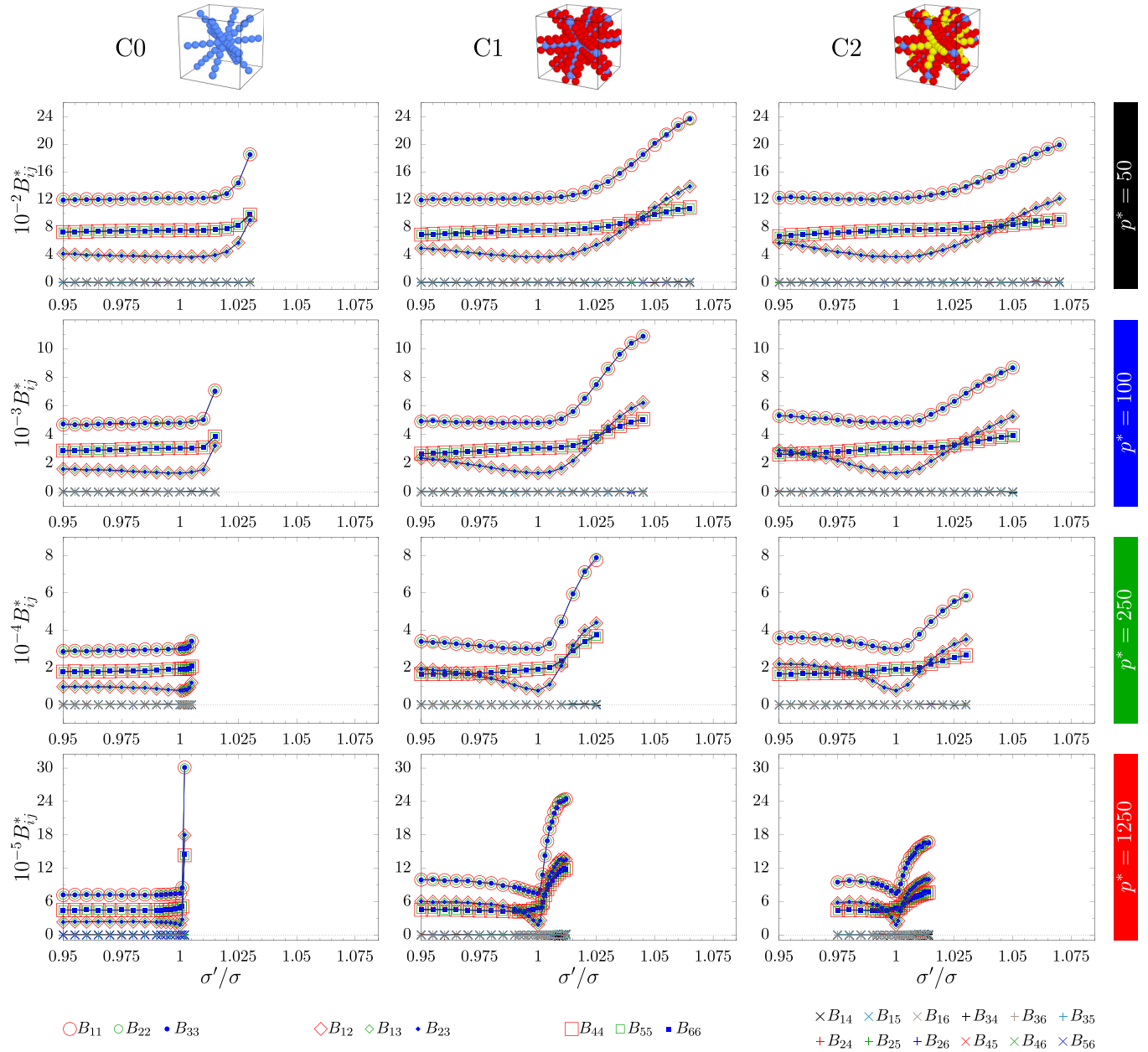
FIG. 3. The components $B_{ij}^* = B_{ij}\beta\sigma^3$ of elastic constant matrix **B**, plotted with respect to σ'/σ. The rows show results for different pressures. The columns show results for systems C0, C1, and C2, which are additionally described by graphical inserts.

elastic constants are similar. This shows the possibility of strengthening or weakening the crystal stiffness only by introducing inclusions in the form of nanochannels in different crystallographic directions. In addition, it is worth emphasizing that the cubic symmetry of the crystals is preserved in both cases.

Another significant conclusion can be drawn from the comparison of the Poisson's ratio in the crystallographic direction [110][1$\bar{1}$0], in which the system of hard spheres shows auxetic properties. In Fig. 6, we can see that when a nanochannel is filled with spheres of a larger diameter than the spheres forming the rest of the crystal, an increase in Poisson's ratio is observed in both systems. However, for the system with four nanochannels (in the [111]-direction and equivalent), the auxetic properties disappear entirely

(for $\sigma'/\sigma > 1.04$), while the system with six nanochannels (in the [110]-direction and equivalent) retains the auxetic properties.

To facilitate the comparison of the results for different systems, it is helpful to present them in a spherical coordinate system like in Fig. 4(b). Insets of Fig. 6 show the surfaces of the minimum values of Poisson's ratio in all crystallographic directions for $\sigma'/\sigma = 1.055$, for systems with six and four nanochannels in comparison with results for the pristine hard sphere crystal ($\sigma'/\sigma = 1.0$). There are no crystallographic directions with a negative Poisson's ratio for a system with four nanochannels. At the same time, it can be seen that the auxetic properties of the system with six nanochannels are still present, although they are weaker than compared to the crystal of hard spheres without nanochannels. Additionally, the value
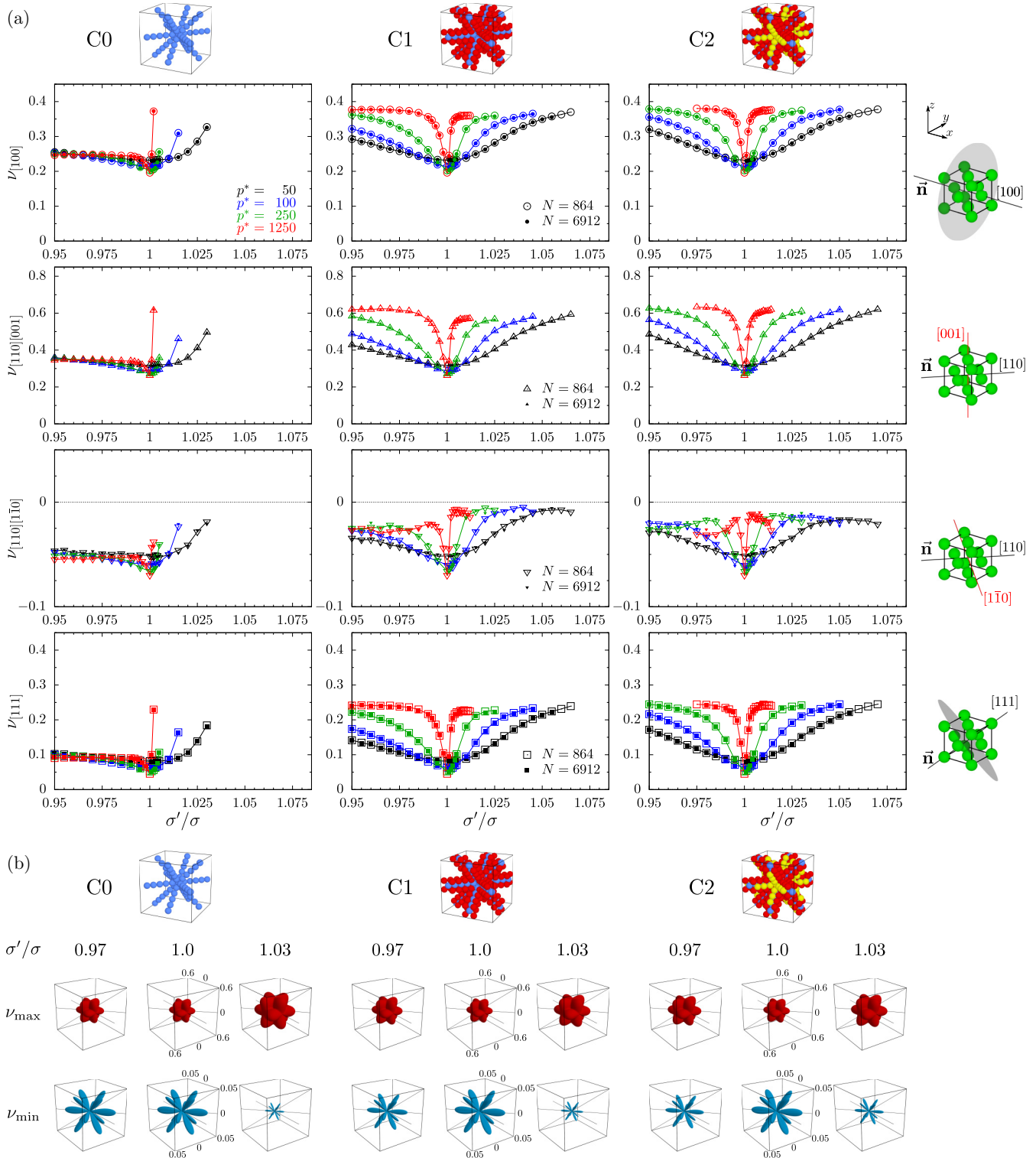
FIG. 4. (a) The Poisson's ratio in main crystallographic directions. Results for systems C0, C1, and C2 (indicated at the top of the figure) are presented in columns. Open symbols represent the results obtained for systems consisting of $N = 864$ particles. Full small symbols describe results for system $N = 6912$ spheres. (b) The absolute value of the minimum negative Poisson's ratio and the maximum value of the Poisson's ratio in all crystallographic directions plotted in spherical coordinates for $p^* = 50$.

of minimum positive Poisson's ratio increases with σ'/σ for both systems in all crystallographic directions.

Remark. Recently, Charbonneau *et al.* [70] published a paper on stability of hard sphere crystals in dimensions between three and ten. The results published there encourage one to study the elastic properties of such models in the context of auxeticity and the influence of "nanochannel" inclusions on their elastic properties.
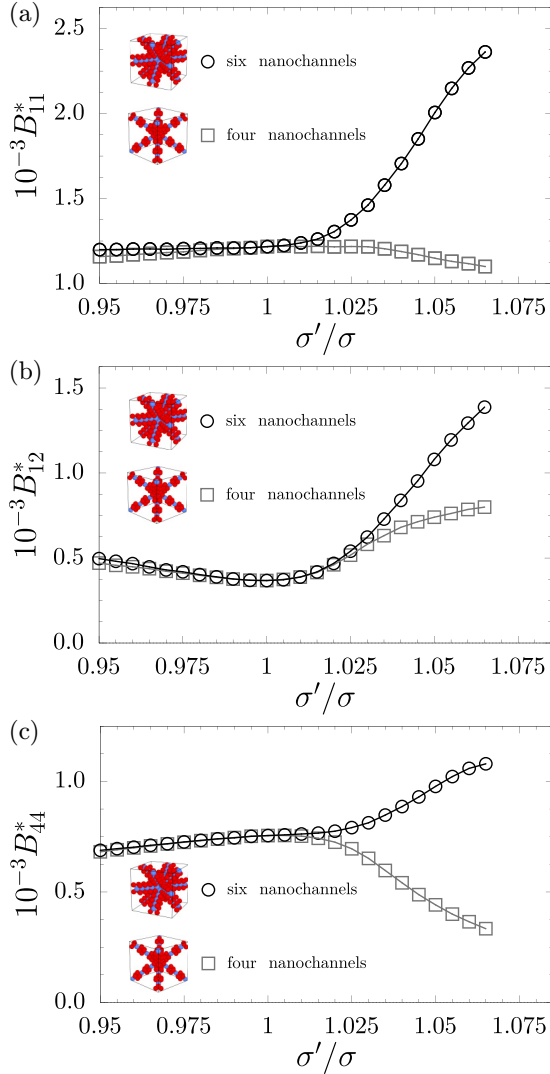
FIG. 5. The elastic constants of system C1 with six nanochannels (in the [110]-direction and equivalent ones) and system C1 with four nanochannels (in the [111]-direction and equivalent ones) at $p^* = 50$. Open circles represent the results obtained in this work. Results of MC simulations are described in open squares from Ref. [62].
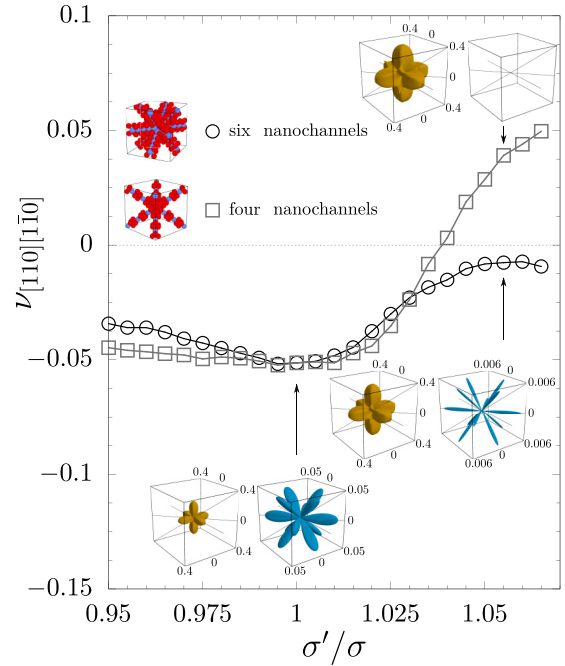

FIG. 6. The Poisson's ratio in the $[110][1\bar{1}0]$-direction of system C1 with six nanochannels (in the [110]-direction and equivalent ones) and system C1 with four nanochannels (in the [111]-direction and equivalent ones) at $p^* = 50$. Open circles represent the results obtained in this work. Results of MC simulations are described in open squares from Ref. [62]. The inserts represent the minimum positive Poisson's ratio (yellow) and the absolute value of the minimum negative Poisson's ratio (blue) in all crystallographic directions for $\sigma'/\sigma = 1.0$ and $\sigma'/\sigma = 1.055$.

V. CONCLUSION

The elastic properties of the hard sphere crystal with six nanochannels filled with spheres of another diameter were determined using Monte Carlo simulations. The axes of nanochannels are oriented in the [110]-direction and equivalent ones. Three types of nanoinclusions formed by spheres of different diameters have been studied.

The studies showed that not only the different diameter of inclusion spheres but also the size, shape, and orientation of the inclusion are critical factors in the modification of elastic properties of the cubic crystal. The introduction of inclusions into the pristine hard sphere crystal was found to increase Poisson's ratios. This effect is strongly correlated with the type of inclusion and the difference in sizes of the inclusion spheres and the spheres forming the crystal. Additionally, it was found that filling nanochannels with larger diameter spheres than spheres formed the crystal increased

the values of elastic constants, and enhanced the stiffness of the fcc hard sphere crystal. Comparison of elastic constants of systems with six nanochannels in the [110]-direction and equivalent ones and systems with four nanochannels in the [111]-direction and equivalent ones [62] showed the possibility of enhancing or weakening crystal stiffness, depending on the orientation of the respective nanochannels. One should add that the cubic symmetry is the highest crystalline one. From this point of view, one can pose a question if, within this high symmetry, it is possible to obtain qualitatively different behaviors of elastic properties in the hard sphere system. The present paper gives a positive answer to this question.

Another interesting and important observation concerns the auxetic properties of the studied systems. In particular, the introduction of four nanochannels in the [111]-direction and equivalent ones into the system of hard spheres (in a way to preserve the cubic symmetry) led to the loss of auxetic properties [62]. The present study revealed that the system with six nanochannels oriented in the [110]-direction and equivalent ones retained not only cubic symmetry but also the auxetic properties.

The most important finding of this work is that in a system consisting of only hard spheres by introducing six nanochannel arrays, the effect of strengthening the crystal stiffness can be obtained while also maintaining the crystal's cubic symmetry and auxetic properties.

[1] R. S. Lakes, Foam structures with a negative Poisson's ratio, Science **235**, 1038 (1987).

[2] K. E. Evans, Auxetic polymers: A new range of materials, Endeavour **15**, 170 (1991).

[3] L. D. Landau and E. M. Lifshitz, *Theory of Elasticity* (Pergamon Press, London, UK, 1986).

[4] A. G. Kolpakov, Determination of the average characteristics of elastic frameworks., J. Appl. Math. Mech. **49**, 739 (1985).

[5] R. F. Almgren, An isotropic three-dimensional structure with Poisson's ratio = −1, J. Elast. **15**, 427 (1985).

[6] K. W. Wojciechowski, Constant thermodynamic tension Monte Carlo studies of elastic properties of a two-dimensional system of hard cyclic hexamers, Mol. Phys. **61**, 1247 (1987).

[7] K. W. Wojciechowski, Two-dimensional isotropic model with a negative Poisson ratio, Phys. Lett. A **137**, 60 (1989).

[8] K. W. Wojciechowski and A. C. Brańka, Negative Poisson ratio in a two-dimensional isotropic solid, Phys. Rev. A **40**, 7222 (1989).

[9] R. H. Baughman, J. M. Shacklette, A. A. Zakhidov, and S. Stafstrom, Negative Poisson's ratios as a common feature of cubic metals, Nature (London) **392**, 362 (1998).

[10] A. C. Brańka, D. M. Heyes, and K. W. Wojciechowski, Auxeticity of cubic materials under pressure, Phys. Status Solidi B **248**, 96 (2011).

[11] A. C. Branka, D. M. Heyes, S. Mackowiak, S. Pieprzyk, and K. W. Wojciechowski, Cubic materials in different auxetic regions: Linking microscopic to macroscopic formulations, Phys. Status Solidi B **249**, 1373 (2012).

[12] V. A. Gorodtsov, M. A. Volkov, and D. S. Lisovenko, Out-of-plane tension of thin two-layered plates of cubic crystals, Phys. Status Solidi B **258**, 2100184 (2021).

[13] I. S. Pavlov, S. V. Dmitriev, A. A. Vasiliev, and A. V. Muravieva, Models and auxetic characteristics of a simple cubic lattice of spherical particles, Continuum Mech. Thermodyn. **34**, 1669 (2022).

[14] A. I. Epishina and D. S. Lisovenko, Influence of the crystal structure and type of interatomic bond on the elastic properties of monatomic and diatomic cubic crystals, Mech. Solids **57**, 1344 (2022).

[15] R. Lakes, Negative-Poisson's-ratio materials: Auxetic solids, Annu. Rev. Mater. Res. **47**, 63 (2017).

[16] S. E. Williams, Q. Zhang, C. de Kergariou, and F. Scarpa, Investigating the effect of relative humidity on the mechanics and dynamics of open-cell polyurethane auxetic foams, Phys. Status Solidi B **259**, 2200442 (2022).

[17] P. Verma, C. B. He, and A. C. Griffin, Implications for auxetic response in liquid crystalline polymers: X-ray scattering and space-filling molecular modeling, Phys. Status Solidi B **257**, 2000261 (2020).

[18] Y. Cheng, X. Zhang, Y. Qin, P. Dong, W. Yao, J. Matz, P. M. Ajayan, J. Shen, and M. Ye, Super-elasticity at 4K of covalently crosslinked polyimide aerogels with negative Poisson's ratio, Nat. Commun. **12**, 4092 (2021).

[19] G. Milton, Composite materials with Poisson's ratios close to -1, J. Mech. Phys. Solids **40**, 1105 (1992).

[20] D. M. Kochmann and G. N. Venturini, Homogenized mechanical properties of auxetic composite materials in finite-strain elasticity, Smart Mater. Struct. **22**, 084004 (2013).

[21] N. Novak, M. Vesenjak, G. Kennedy, N. Thadhani, and Z. Ren, Response of chiral auxetic composite sandwich panel to fragment simulating projectile impact, Phys. Status Solidi B **257**, 1900099 (2020).

[22] J. I. Lipton, R. MacCurdy, Z. Manchester, L. Chin, D. Cellucci, and D. Rus, Handedness in shearing auxetics creates rigid and compliant structures, Science **360**, 632 (2018).

[23] T. C. Lim, *Auxetic Materials and Structures* (Springer, Singapore, 2015).

[24] S. Bao, X. Ren, Y. J. Qi, H. R. Li, D. Han, W. Li, C. Luo, and Z. Z. Song, Quasi-static mechanical properties of a modified auxetic re-entrant honeycomb metamaterial, Phys. Status Solidi B **259**, 2200270 (2022).

[25] D. T. Ho, S. Y. Kim, and U. Schwingenschlögl, Graphene origami structures with superflexibility and highly tunable auxeticity, Phys. Rev. B **102**, 174106 (2020).

[26] K. Yuan, Y. Zhao, M. Li, and Y. Liu, Predicting an ideal 2D carbon nanostructure with negative Poisson's ratio from first principles: implications for nanomechanical devices, Carbon Lett. **31**, 1227 (2021).

[27] K. Bertoldi, V. Vitelli, J. Christensen, and M. van Hecke, Flexible mechanical metamaterials, Nat. Rev. Mater. **2**, 17066 (2017).

[28] T.-C. Lim, *Mechanics of Metamaterials with Negative Parameters* (Springer: Singapore, 2020).

[29] J. N. Grima-Cornish, R. Cauchi, D. Attard, R. Gatt, and J. N. Grima, Smart honeycomb "mechanical metamaterials" with tunable Poisson's ratios, Phys. Status Solidi B **257**, 1900707 (2020).

[30] F. Usta, F. Scarpa, H. S. Turkmen, P. Johnson, A. W. Perriman, and Y. Y. Chen, Multiphase lattice metamaterials with enhanced mechanical performance, Smart Mater. Struct. **30**, 025014 (2021).

[31] K. K. Dudek, J. A. I. Martinez, G. Ulliac, and M. Kadic, Micro-scale auxetic hierarchical mechanical metamaterials for shape morphing, Adv. Mater. **34**, 2110115 (2022).

[32] K. K. Dudek, J. A. I. Martinez, G. Ulliac, L. Hirsinger, L. Wang, V. Laude, and M. Kadic, Micro-scale mechanical metamaterial with a controllable transition in the Poisson's ratio and band gap formation, Adv. Mater. **35**, 2210993 (2023).

[33] D. Tahir, M. Zhang, and H. Hu, Auxetic materials for personal protection: A review, Phys. Status Solidi B **259**, 2200324 (2022).

[34] W. G. Hoover and C. G. Hoover, Searching for auxetics with DYNA3D and ParaDyn, Phys. Status Solidi B **242**, 585 (2005).

[35] I. Shufrin, E. Pasternak, and A. V. Dyskin, Effective properties of layered auxetic hybrids, Composite Structures **209**, 391 (2019).

[36] E. A. Korznikova, K. Zhou, L. K. Galiakhmetova, E. G. Soboleva, A. A. Kudreyko, and S. V. Dmitriev, Partial auxeticity of laterally compressed carbon nanotube bundles, Phys. Status Solidi (RRL) **16**, 2100189 (2022).

[37] J. N. Grima and K. E. Evans, Auxetic behavior from rotating squares, J. Mater. Sci. Lett. **19**, 1563 (2000).

[38] E. Chetcuti, B. Ellul, E. Manicaro, J.-P. Brincat, D. Attard, R. Gatt, and J. N. Grima, Modeling auxetic foams through semi-rigid rotating triangles, Phys. Status Solidi B **251**, 297 (2014).

[39] L. Rothenburg, A. A. Berlin, and R. J. Bathurst, Microstructure of isotropic materials with negative Poisson's ratio, Nature (London) **354**, 470 (1991).

[40] H. Kimizuka, H. Kaburaki, and Y. Kogure, Mechanism for negative Poisson ratios over the $\alpha-\beta$ transition of cristobalite, SiO_2: A molecular-dynamics study, Phys. Rev. Lett. **84**, 5548 (2000).

[41] I. Shufrin, E. Pasternak, and A. V. Dyskin, Hybrid materials with negative Poisson's ratio inclusions, Int. J. Eng. Sci. **89**, 100 (2015).

[42] B. D. Caddock and K. E. Evans, Microporous materials with negative Poisson's ratios. I. microstructure and mechanical properties, J. Phys. D: Appl. Phys. **22**, 1877 (1989).

[43] S. Hirotsu, Elastic anomaly near the critical point of volume phase transition in polymer gels, Macromolecules **23**, 903 (1990).

[44] X. Xu, Q. Zhang, M. Hao, Y. Hu, Z. Lin, L. Peng, T. Wang, X. Ren, C. Wang, Z. Zhao, C. Wan, H. Fei, L. Wang, J. Zhu, H. Sun, W. Chen, T. Du, B. Deng, G. J. Cheng, I. Shakir *et al.*, Double-negative-index ceramic aerogels for thermal superinsulation, Science **363**, 723 (2019).

[45] T. Shepherd, K. Winwood, P. Venkatraman, A. Alderson, and T. Allen, Validation of a finite element modeling process for auxetic structures under impact, Phys. Status Solidi B **257**, 1900197 (2020).

[46] K. V. Tretiakov and K. W. Wojciechowski, Poisson's ratio of the fcc hard sphere crystal at high densities, J. Chem. Phys. **123**, 074509 (2005).

[47] K. V. Tretiakov and K. W. Wojciechowski, Elastic properties of soft sphere crystal from Monte Carlo simulations, J. Phys. Chem. B **112**, 1699 (2008).

[48] P. M. Piglowski, K. W. Wojciechowski, and K. V. Tretiakov, Partial auxeticity induced by nanoslits in the Yukawa crystal, Phys. Status Solidi (RRL) **10**, 566 (2016).

[49] K. V. Tretiakov, P. M. Piglowski, and K. W. Wojciechowski, Auxeticity modifications and unit cell doubling in Yukawa fcc crystals with [001]-nanochannels filled by hard spheres, Smart Mater. Struct. **32**, 025008 (2023).

[50] J. P. Hansen and I. R. McDonald, *Theory of Simple Liquids* (Academic Press, Amsterdam, The Netherlands, 2006).

[51] M. P. Allen and D. J. Tildesley, *Computer Simulations of Liquids* (Clarendon Press, Oxford, UK, 1987).

[52] D. Frenkel and A. J. C. Ladd, Elastic constants of hard-sphere crystals, Phys. Rev. Lett. **59**, 1169 (1987).

[53] K. J. Runge and G. V. Chester, Monte Carlo determination of the elastic constants of the hard-sphere solid, Phys. Rev. A **36**, 4852 (1987).

[54] E. Velasco and P. Tarazona, Elastic properties of hard-sphere crystal, Phys. Rev. A **36**, 979 (1987).

[55] H. Xu and M. Baus, Elastic-constants of the hard-sphere solid from density-functional theory, Phys. Rev. A **38**, 4348 (1988).

[56] M. V. Jaric and U. Mohanty, Density-functional theory of elastic moduli: Hard-sphere and Lennard-Jones crystals, Phys. Rev. B **37**, 4441 (1988).

[57] O. Farago and Y. Kantor, Fluctuation formalism for elastic constants in hard-spheres-and-tethers systems, Phys. Rev. E **61**, 2478 (2000).

[58] S. Pronk and D. Frenkel, Large difference in the elastic properties of fcc and hcp hard-sphere crystals, Phys. Rev. Lett. **90**, 255501 (2003).

[59] J. W. Narojczyk, K. W. Wojciechowski, K. V. Tretiakov, J. Smardzewski, F. Scarpa, P. M. Piglowski, M. Kowalik, A. R. Imre, and M. Bilski, Auxetic properties of a f.c.c. crystal of hard spheres with an array of [001]-nanochannels filled by hard spheres of another diameter, Phys. Status Solidi B **256**, 1800611 (2019).

[60] J. W. Narojczyk, M. Bilski, J. N. Grima, P. Kedziora, D. Morozow, M. Rucki, and K. W. Wojciechowski, Removing auxetic properties in f.c.c. hard sphere crystals by orthogonal nanochannels with hard spheres of another diameter, Materials **15**, 1134 (2022).

[61] J. W. Narojczyk, K. V. Tretiakov, and K. W. Wojciechowski, Rise of the Poisson's ratio in f.c.c. hard sphere crystals with the narrowest orthogonal nanochannels filled by hard spheres of another diameter, Comput. Methods Sci. Technol. **28**, 61 (2022).

[62] J. W. Narojczyk, K. V. Tretiakov, and K. W. Wojciechowski, Poisson's ratio of f.c.c. hard-sphere crystals with cubic supercells containing four nanochannels filled by hard spheres of another diameter, Phys. Status Solidi B **259**, 2200464 (2022).

[63] R. Ali, M. R. Saleem, M. Roussey, J. Turunen, and S. Honkanen, Fabrication of buried nanostructures by atomic layer deposition, Sci. Rep. **8**, 15098 (2018).

[64] K. W. Wojciechowski, K. V. Tretiakov, and M. Kowalik, Elastic properties of dense solid phases of hard cyclic pentamers and heptamers in two dimensions, Phys. Rev. E **67**, 036121 (2003).

[65] M. Parrinello and A. Rahman, Polymorphic transitions in single crystals: A new molecular dynamics method, J. Appl. Phys. **52**, 7182 (1981).

[66] M. Parrinello and A. Rahman, Strain fluctuations and elastic constants, J. Chem. Phys. **76**, 2662 (1982).

[67] J. H. Weiner, *Statistical Mechanics of Elasticity* (Wiley, New York, USA, 1983).

[68] S. P. Tokmakova, Stereographic projections of Poisson's ratio in auxetic crystals, Phys. Status Solidi B **242**, 721 (2005).

[69] J. F. Nye, *Physical Properties of Crystals, Their Representation by Tensors and Matrices* (Clarendon Press, Oxford, UK, 1957).

[70] P. Charbonneau, C. M. Gish, R. S. Hoy, and P. K. Morse, Thermodynamic stability of hard sphere crystals in dimensions 3 through 10, Eur. Phys. J. E **44**, 101 (2021).